Numerical Analyses on Multi-DOF Ultrasonic Motor

- Development of Analysis Method and Results -

Kenjiro Takemura, Takashi Maeno

Abstract— **A multi-DOF ultrasonic motor developed in our previous study has significant potentials for dexterous actuation. The ultrasonic motor provides multi-DOF rotation of a spherical rotor using three natural vibrations of a bar-shaped stator. In this paper, numerical analyses on the multi-DOF ultrasonic motor are conducted. First, a forward model of multi-DOF ultrasonic motor is developed considering the frictional condition between the rotor/stator. Using the forward model, driving state of the multi-DOF ultrasonic motor under arbitrary combination of vibrations is clarified. Second, an inverse model of the multi-DOF ultrasonic motor is also developed. The inverse model is constructed using experienced knowledge about ultrasonic motor and neural network technique. An appropriate input for the multi-DOF ultrasonic motor with regard to arbitrary rotational axis is estimated using the inverse model. The proposed models are available not only for our motor but for all multi-DOF ultrasonic motors.**

Keywords— **Ultrasonic motor, Muli-DOF, Simulation, Neural Network.**

I. Introduction

ROBOTS are now widely used in the field of industry, amusement, extreme work, medicine, and so on. In other words, target of robots has much more relation to our lives in last decade, and some of them are handled not only by specialists but also by nonprofessionals for engineering. Generating dexterous motion like human beings is one of the most important subjects in the field of robotics. Dexterous multi-DOF motion is generally generated by combining single-DOF motions of electromagnetic motors with reduction dears. In this case, however, it is difficult to construct a compact multi-DOF motion unit. To solve the issue, some multi-DOF actuators have been proposed and developed, which can generate multi-DOF motion using only single stators. As examples of multi-DOF electromagnetic actuator, Roth *et al.* proposed a three-DOF variable reluctance spherical wrist motor [1], and Yano developed a spherical stepping motor [2]. Structures of their motors, however, are so complicated that they cannot be compact.

On the other hand, ultrasonic motors have excellent characteristics such as high torque at low speed, high stationary limiting torque, absence of electromagnetic radiation, quiet, and simplicity of design. Therefore, multi-DOF actuators extending the principle of ultrasonic motors have been proposed as follows: Bansevicius developed a piezoelectric multi-DOF actuator [3]. Amano *et al.* developed a multi-DOF ultrasonic actuator [4]. Toyama constructed a spherical ultrasonic motor [5]. Sasae *et al.* developed a spherical actuator [6]. Authors have also developed a new type of multi-DOF ultrasonic motor [7], which generates multi-DOF rotation of a spherical rotor using three natural vibration modes of a bar-shaped stator.

For ultrasonic motors generally have great features as mentioned above, the multi-DOF ultrasonic motors [3]-[7] have potentials to take place of general multi-DOF units of single-DOF electromagnetic motors. To put them into practical, numerical analyses on the ultrasonic motors must be conducted in order to clarify the input/output relationships. At this point, we propose the forward and inverse models of multi-DOF ultrasonic motors in the present paper.

There have been proposed some analysis methods for practical single-DOF ultrasonic motors. Maeno reported a "finite element analysis of the rotor/stator contact in ring-type ultrasonic motor" [8] and a "contact analysis of traveling wave type ultrasonic motor considering stick/slip condition" [9]. Kurosawa reported an "efficiency of ultrasonic motor using traveling wave" [10]. Although the methods are suitable for the single-DOF ultrasonic motors, they are not for the multi-DOF ones, because they have been calculated under the assumption that the rotational axis is known. In case of the multi-DOF ultrasonic motors, rotational axis is arbitrary according to a combination of vibration modes. Furthermore, parameters, such as frequency, amplitude, and phase of vibrations, have independent non-linear characteristics and their combinations are redundant against the rotor motion.

So, we propose first a new type of numerical forward model, which has ability to identify the rotational axis of the spherical rotor under the arbitrary combination of vibration modes. Then, a number of input/output pairs of multi-DOF ultrasonic motor are obtained using the forward model. Finally, an inverse model based on a neural network technique is made and the neural network is trained using the input/output pairs to be

K. Takemura and T. Maeno are with the Department of Mechanical Engineering, Keio University, Yokohama, Japan. E-mail: kenjiro@mmm-keio.net (takemura), maeno@mech.keio.ac.jp (maeno).

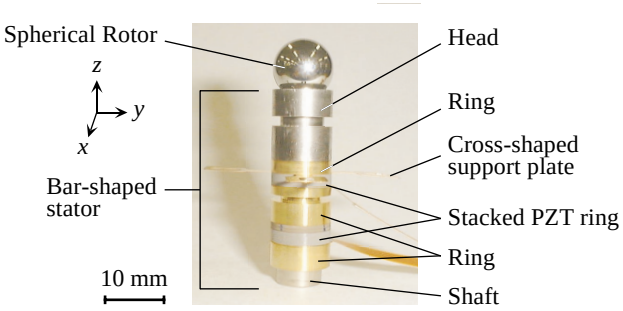

Fig. 1. Multi-DOF ultrasonic motor

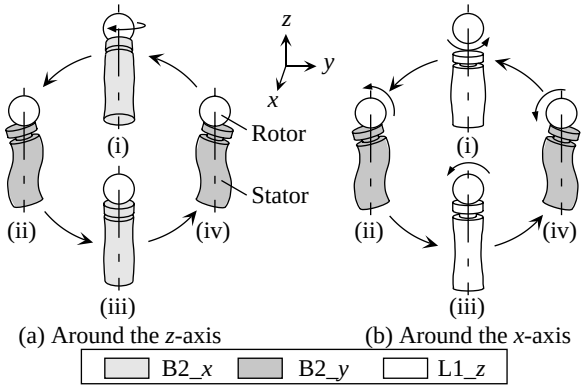

Fig. 2. Driving principle

the inverse model of multi-DOF ultrasonic motor.

In the present paper, outline of the hardware, multi-DOF ultrasonic motor, is briefly described in chapter II. Then, the forward and inverse models of multi-DOF ultrasonic motor are described in chapter III and IV, respectively. In chapter V, conclusions of this study are described.

II. Multi-dof Ultrasonic Motor

The multi-DOF ultrasonic motor we developed [7] is shown in Fig. 1. The ultrasonic motor consists of a bar-shaped stator and a spherical rotor. The diameter, height, and mass of the stator are 10.0 mm, 31.8 mm, and 16.9 g, respectively. Multi-DOF rotation of the rotor like human wrist joint is generated using two bending vibrations and a longitudinal vibration of the stator, whose natural frequencies are designed to correspond. Basal driving principles of the ultrasonic motor are shown in Fig. 2. The rotor is rotated around the z-axis by the rotor/stator frictional force, when the two orthogonal bending vibrations are excited on the stator with quarter cycle interval as shown in Fig. 2 (a). On the other hand, the rotor is rotated around the x-(y-)axis, when the bending and longitudinal vibrations are combined as shown in Fig. 2 (b). Furthermore, a rotation around arbitrary axis is generated when the vibrations are appropriately combined.

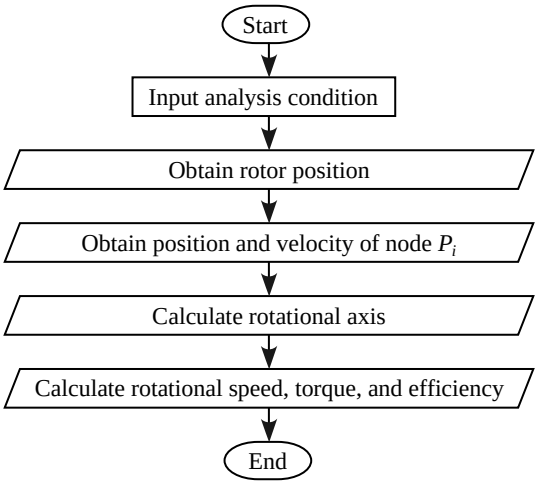

Fig. 3. Flowchart of forward model

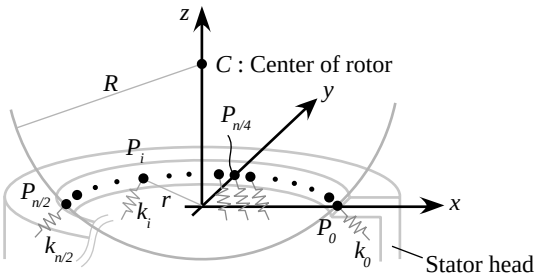

Fig. 4. Numrical model for multi-DOF ultrasonic motor

III. Forward Model

Since the multi-DOF ultrasonic motor can potentially generates the motion like human wrist joint, it is difficult to estimate which axis the rotor rotates around when three vibrations are arbitrary combined. It is also difficult to estimate the rotational speed and torque. Although there have been some researches on numerical simulation for practical single-DOF ultrasonic motors [8]-[10], the simulations are not available for the multi-DOF ultrasonic motor because of a following reason. The previous method works under an assumption that the rotational axis of rotor is mechanically fixed, however, it is not fixed in case of the multi-DOF ultrasonic motors. So, we develop a new type of analysis method using forward model for multi-DOF ultrasonic motor.

A. Analysis Method for Forward Model

The natural vibrations in the x-, y-, and z-direction are used in the multi-DOF ultrasonic motor. A method for estimating the driving characteristics of the rotor is proposed as follows. The flowchart of proposed analysis method is shown in Fig. 3.

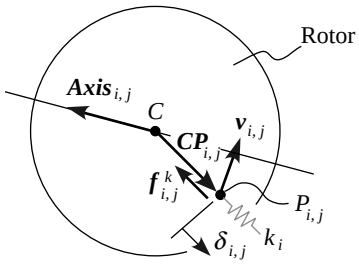

Fig. 5. Node $P_{i,j}$ and its kinematics' vectors

A.1 Modeling and parameters

Since the ultrasonic motor is a frictionally driven motor, contact condition between the rotor/stator significantly influences the driving characteristic. So, the contact area between the rotor/stator is modeled using nodes P_i and linear spring k_i as shown in Fig. 4, where n is a total number of the nodes. The directions of each spring k_i are the same as those of vector $\boldsymbol{CP}_i$. A cycle of vibration is divided to m steps. Parameters for the analysis are as follows.

f : frequency of vibrations
A_ξ : amplitude of vibration in ξ-direction
f_ξ : phase of vibration in ξ-direction
$\boldsymbol{F}$: pre-load between the rotor/stator

A.2 Rotor position and nodes' kinematics

The position of the center of the rotor is calculated considering the balance of spring force and external pre-load between the rotor/stator. Then, positions $\boldsymbol{P}_{i,j}$ and velocities $\boldsymbol{v}_{i,j}$ of ith node at jth step are calculated using the shapes of each vibration mode obtained by the finite element analysis.

A.3 Rotational axis

Driving torque $\boldsymbol{\tau}_{i,j}$ of ith node at jth step are obtained using the positions $\boldsymbol{P}_{i,j}$ and velocities $\boldsymbol{v}_{i,j}$ as follows. Kinematics' vectors at jth step with regard to the rotor and node P_i are shown in Fig. 5, where $\boldsymbol{Axis}_{i,j}$ is a rotational axis by the torque $\boldsymbol{\tau}_{i,j}$, $\boldsymbol{\delta}_{i,j}$ is the decline of node P_i against the rotor, and $\boldsymbol{f^k}_{i,j}$ is the spring force. If it is assumed that the rotor is stationary and the stator always slips against the rotor, the node P_i provides a frictional force $\mu\boldsymbol{f^k}_{i,j}$ in the direction of velocity $\boldsymbol{v}_{i,j}$, where μ is a dynamic friction coefficient. Then, the torque $\boldsymbol{\tau}_{i,j}$ is defined by

$$\boldsymbol{\tau}_{i,j} = \mu\boldsymbol{f^k}_{i,j} \times \boldsymbol{CP}_{i,j} = \mu\boldsymbol{k}_i\boldsymbol{\delta}_{i,j} \times \boldsymbol{CP}_{i,j} \quad (1)$$

A driving torque $\boldsymbol{T}$ is obtained by averaging the sum of the torque $\boldsymbol{\tau}_{i,j}$ of all nodes throughout a cycle. As a result, the direction and magnitude of the torque $\boldsymbol{T}$ represent the direction of the rotational axis and the maximum torque of the rotor, respectively.

TABLE I
SIMULATED CONDITIONS AND RESULTS

No.		B2_x	B2_y	L1	Rot. axis	Rot. speed [rpm]
(1)	Amp. [μm]	1	1	0	$\begin{pmatrix}0\\0\\1\end{pmatrix}$	504
	Phase [deg]	0	90	0		
(2)	Amp. [μm]	1	0	1	$\begin{pmatrix}0\\1\\0\end{pmatrix}$	361
	Phase [deg]	0	0	90		
(3)	Amp. [μm]	1	0.8	1	$\begin{pmatrix}-0.422\\0.741\\-0.523\end{pmatrix}$	314
	Phase [deg]	0	30	60		

A.4 Rotational speed, torque and efficiency

The rotational speed, output torque and efficiency around the rotational axis derived above are calculated. If the angular velocity ω is known, an output torque $\tau^{out}_{i,j}$ and a power loss by friction $w^{loss}_{i,j}$ is defined by

$$\tau^{out}_{i,j} = \mu f^k_{i,j} \cdot \left|\frac{v^t_{i,j}}{v_{i,j}}\right| \cdot R_{i,j} \cdot sgn(v^t_{i,j} - \omega R_{i,j}) \quad (2)$$

$$w^{loss}_{i,j} = \mu f^k_{i,j} \cdot \left|\frac{v^t_{i,j}}{v_{i,j}}\right| \cdot \left|v^t_{i,j} - \omega R_{i,j}\right| \quad (3)$$

where, $v^t_{i,j}$ and $R_{i,j}$ are a tangential velocity around the rotational axis and a distance from the rotational axis of node P_i, respectively. A total output torque T^{out} and a total power loss by friction W^{loss} are obtained as a summation of the averaged output torque and the power loss by friction at each step. Efficiency is calculated by

$$\eta = \frac{T^{out} \cdot \omega}{T^{out} \cdot \omega + W^{loss}} \quad (4)$$

A T-N curve (relationship between the output torque and rotational speed) and a T-η curve (relationship between the output torque and efficiency) are obtained by sweeping the angular velocity ω.

B. Results of Forward Model

Driving characteristics of the multi-DOF ultrasonic motor are calculated using the proposed method. The numbers of nodes, steps and natural frequencies of the modes are 360, 100 and 40 kHz, respectively. Other analytical conditions and simulated results are shown in Table I, where the rotational axes are normalized. When the two bending vibrations are combined, the rotational axis agrees with the z-axis, and when the longitudinal mode and the bending mode in the z-x plane are combined, it agrees with the y-axis as shown in Table I (1) and (2). The results agree well with the theoretical driving axis as shown in Fig. 2. A rotational axis obtained in condition (3) means that the mixture of vibration modes occurred when phase

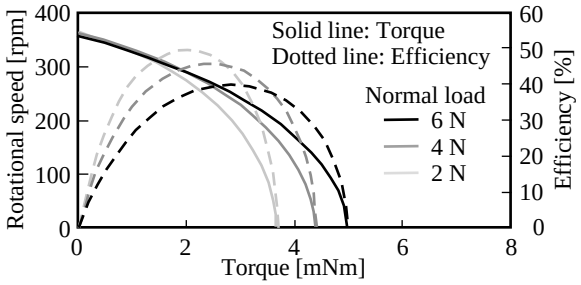

Fig. 6. Simulated T-N and T-η curves

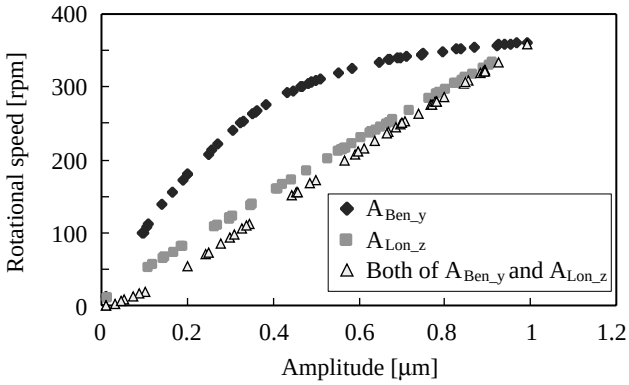

(a) Rotational speed against amplitude

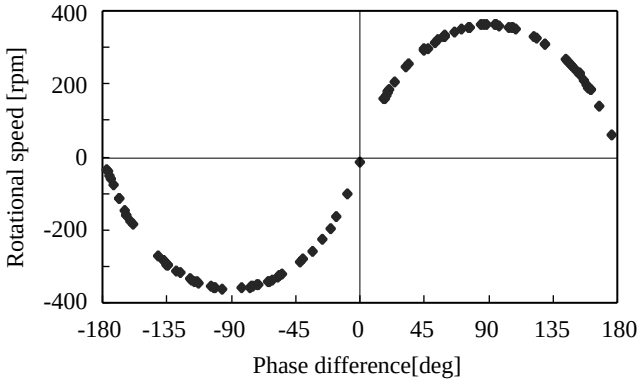

(b) Rotational speed against phase difference

Fig. 7. Simulated rotational speed against each parameter (Rotation around the x-axis)

differences of each modes are not equal to 0 or 180 deg. Simulated T-N curve and T-η curve are shown in Fig. 6. The rotational speed decreases as the torque increases. The efficiency shows a parabola characteristic. The maximum torque under the simulated conditions is about 5 mNm. The result agrees with the experimental results obtained in our previous study [7]. Furthermore, effects of each parameter for the rotational speed are simulated as partly shown in Fig. 7. Each parameter has non-linear effects against the driving state. Still more, there you can see a redundancy of the combination of parameters, i.e., the same driving state can be obtained under several conditions.

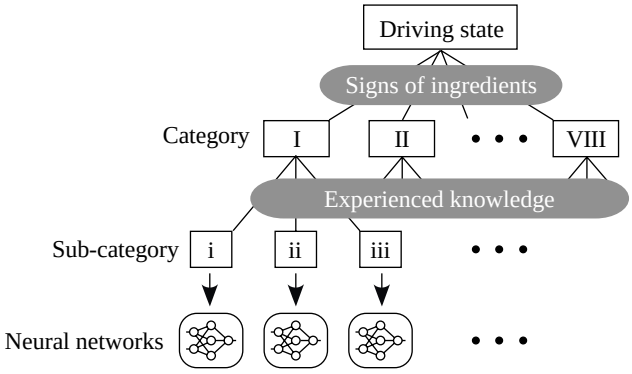

Fig. 8. Constructing process for inverse model

IV. Inverse Model

In order to make the multi-DOF ultrasonic motor practical, it is necessary to construct a control methodology. Therefore, we propose an inverse model of the multi-DOF ultrasonic motor using neural network technique. There have been reported some research on controlling ultrasonic motors with neural network controller [11], however, they have only dealt with the case of single operating parameter. In the inverse model proposed bellow, all of the potential operating parameters for the multi-DOF ultrasonic motor are considered in order to generate a rotation of the rotor around desired rotational axis.

A. Model for Inverse Model

The parameters for multi-DOF ultrasonic motor have non-linear and redundant characteristics against the driving state as mentioned in the section III-B. It is difficult to obtain its inverse model directly. So, we propose a method with three-step process to construct the inverse model as shown in Fig. 8.

A.1 Classification

The driving state of the rotor is expressed using a rotational speed $\boldsymbol{N}$. The direction of $\boldsymbol{N}$ represents the rotational axis. Each ingredient represents rotational speed around each axis of coordinates. We have introduced a normalized rotational speed $\boldsymbol{N^0}$ to make the issue simple. $\boldsymbol{N^0}$ is defined by dividing $\boldsymbol{N}$ by maximum value of the absolute ingredients.

We classify the driving state into 24 classes. First, the driving state is divided into eight categories according to the combination of signs of each ingredient of $\boldsymbol{N^0}$. As a result, an order of phases for each vibration is determined for each category. Next, each category is divided into three sub-categories according to an experienced knowledge; such as the phase difference between the combined vibrations should be quarter cycle in order to make the efficiency of rotation around the axis of coordinate high. Namely, the

TABLE II

COMBINATION OF PHASES AND AMPLITUDES FOR EACH CLASS

Class ID	Cat.	Sub-cat.	N^0			Maximum ingredient	Phase [rad]			Relative amplitude		
			N^0_x	N^0_y	N^0_z		ϕ_{Ben_x}	ϕ_{Ben_y}	ϕ_{Lon_z}	$A^r_{Ben\_x}$	$A^r_{Ben\_y}$	$A^r_{Lon\_z}$
1		(i)				$\|N^0_x\|$	-π/2~0	π/2	0	0~3	1	1
2	I	(ii)	+	+	-	$\|N^0_y\|$	0	π/2~π	π/2	1	0~3	1
3		(iii)				$\|N^0_z\|$	0	π/2	0~π/2	1	1	0~3
4		(i)				$\|N^0_x\|$	π/2~π	π/2	0	0~3	1	1
5	II	(ii)	+	-	+	$\|N^0_y\|$	π/2	0~π/2	0	1	0~3	1
6		(iii)				$\|N^0_z\|$	π/2	0	-π/2~0	1	1	0~3
7		(i)				$\|N^0_x\|$	0~π/2	π/2	0	0~3	1	1
8	III	(ii)	+	-	-	$\|N^0_y\|$	π/2	π/2~π	0	1	0~3	1
9		(iii)				$\|N^0_z\|$	0	π/2	-π/2~0	1	1	0~3
10		(i)				$\|N^0_x\|$	0~π/2	0	π/2	0~3	1	1
11	IV	(ii)	-	+	+	$\|N^0_y\|$	0	-π/2~0	π/2	1	0~3	1
12		(iii)				$\|N^0_z\|$	π/2	0	π/2~π	1	1	0~3
13		(i)				$\|N^0_x\|$	-π/2~0	0	π/2	0~3	1	1
14	V	(ii)	-	+	-	$\|N^0_y\|$	0	0~π/2	π/2	1	0~3	1
15		(iii)				$\|N^0_z\|$	0	π/2	π/2~π	1	1	0~3
16		(i)				$\|N^0_x\|$	π/2~π	0	π/2	0~3	1	1
17	VI	(ii)	-	-	+	$\|N^0_y\|$	π/2	-π/2~0	0	1	0~3	1
18		(iii)				$\|N^0_z\|$	π/2	0	0~π/2	1	1	0~3
19		(i)				$\|N^0_x\|$	-π~-π/2	π/2	0	0~3	1	1
20	VII	(ii)	+	+	+	$\|N^0_y\|$	0	-π~-π/2	π/2	1	0~3	1
21		(iii)				$\|N^0_z\|$	π/2	0	-π~-π/2	1	1	0~3
22		(i)				$\|N^0_x\|$	π/2~π	-π/2	0	0~3	1	1
23	VIII	(ii)	-	-	-	$\|N^0_y\|$	0	π/2~π	-π/2	1	0~3	1
24		(iii)				$\|N^0_z\|$	-π/2	0	π/2~π	1	1	0~3

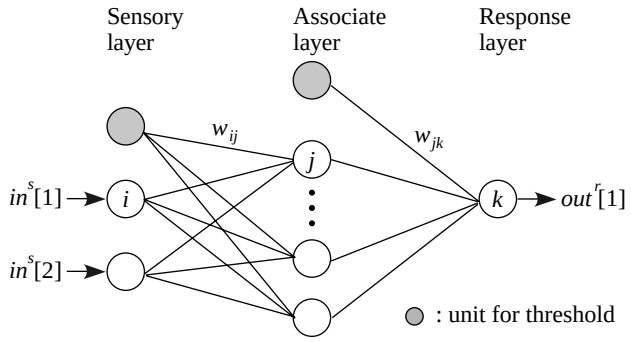

Fig. 9. Structure of neural network

phase difference between the combined vibrations for maximum ingredient of $\boldsymbol{N^0}$ is made to be quarter cycle. Then, ranges of phases and relative amplitudes of the vibrations are determined.

Table II shows the combinations of phases and amplitudes for each class. The classification process determines the phases and relative amplitudes of vibrations except for one vibration. Namely, The experienced knowledge solves the problem of redundancy.

A.2 Neural network

The phase and relative amplitude of a certain vibration are not decided yet. So, we adopt neural network technique for dealing with the non-linear relationship between the undecided parameters and $\boldsymbol{N^0}$. Structure of the neural network is shown in Fig. 9. Two neural networks for the phase and amplitude, respectively, are used. Outline of the network is given as follows:

Sensory layer : Inputs, $in^s[i]$, are the ingredients of $\boldsymbol{N^0}$. Outputs, $out^s[i]$, are defined by

$$out^s[i] = \frac{1}{1+\exp(-in^s[i])} \tag{5}$$

where, i is a number of unit in sensory layer.

Associate layer : Inputs, $in^a[j]$, and outputs, $out^a[j]$, are defined by

$$in^a[j] = \sum_i (w_{ij} out^s[i]) + \theta_j \tag{6}$$

$$out^a[j] = \frac{1}{1+\exp(-in^a[j])} \tag{7}$$

where, w_{ij} is a connective weight between sensory/associate layers, θ_j is a threshold value for the unit in associate layer and j is a number of unit in associate layer.

Response layer : Inputs, $in^r[k]$, and outputs, $out^r[k]$ are defined by

$$in^r[k] = \sum_j (w_{jk} out^a[j]) + \theta_k \tag{8}$$

$$out^r[k] = in^r[k] \tag{9}$$

where, w_{jk} is a connective weight between associate/response layers, θ_k is a threshold value for the unit in response layer and k is a number of unit in response layer.

A.3 Training

Teacher signals for training the neural networks are obtained using the forward model mentioned in chapter III. Connective weights of the neural networks are trained according to the error back propagation algorithm [11] using the teacher signals. However, ranges of the undecided parameters are encoded to be from 0 to 1.

B. Results of Inverse Model

Relationships between the normalized rotational speed $\boldsymbol{N^0}$ and the undecided parameters in Table II are trained using the neural network and error back propagation technique. Namely, relationships between the $\boldsymbol{N^0}$ as inputs and undecided phase and amplitude as outputs are trained. The training conditions are as follows: numbers of teacher signals, training cycle and units in associate layer are 1000, 50000 and 5, respectively. Initial connective weights are set to be random from -3 to 3, and a training rate is 0.5. Fig. 10 shows the relationships between the teacher signals and outputs from trained neural network in case of class 1. The undecided parameters are respectively well trained. The errors between teacher signals and outputs are within 0.5 % of full scale. The neural

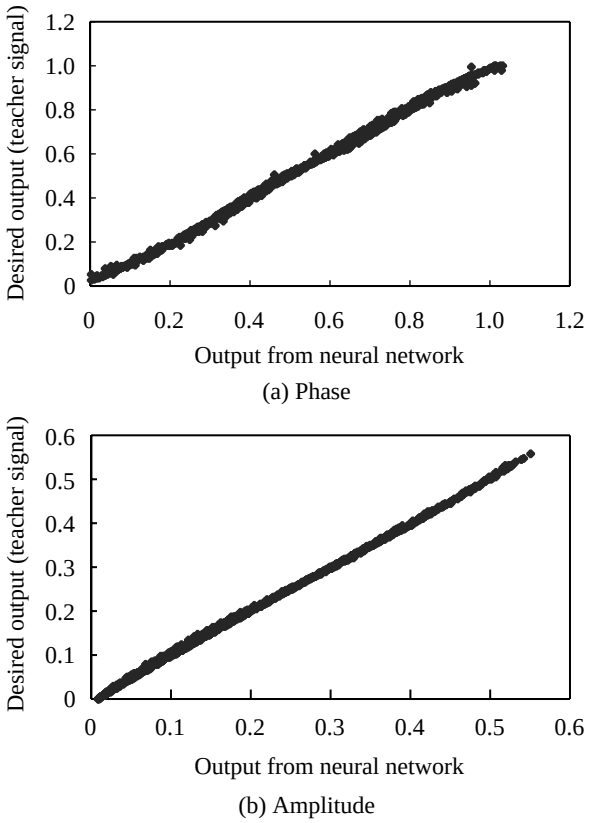

Fig. 10. Results for nural network training

networks for other classes are successfully trained, too. All the parameters for the multi-DOF ultrasonic motor are now determined. Then, appropriate inputs for the multi-DOF ultrasonic motor with regard to arbitrary rotational axis of the rotor are successfully obtained using the inverse model.

V. Conclusions

The methods for analyzing characteristics of the multi-DOF ultrasonic motors have been proposed in this paper. First, the forward model of the multi-DOF ultrasonic motor is developed considering the frictional condition between the rotor/stator. The forward model successfully provides the ability to estimate driving states of the multi-DOF ultrasonic motor even if the combination of vibrations are arbitrary. Second, the inverse model of the multi-DOF ultrasonic motor is also developed. The inverse model is constructed with experienced knowledge about ultrasonic motors and neural network technique. Using the inverse model, an appropriate input for a desired driving can be obtained. The analysis methods proposed in this paper are available not only for our motor but for all multi-DOF ultrasonic motors.

Future study focuses on constructing a controller for multi-DOF ultrasonic motor using the proposed models, on control experiment, and on redesigning the rotor/stator contact condition to increase output torque. Then, the multi-DOF ultrasonic motor presents a dexterous motion for robots.

References

[1] R. Roth, and K-M. Lee, *Design Optimization of a Three Degrees-of-Freedom Variable Reluctance Spherical Wrist Motor*, Trans. ASME J. Engineering for Industry, Vol. 117, pp. 378-388, 1995.

[2] T. Yano *et al.*, *Basic Characteristics of the Developed Spherical Stepping Motor*, Proc. 1999 IEEE/RSJ Int. Conf. Intelligent Robots and Systems, Vol. 3, pp. 1393-1398, 1999.

[3] R. Bansevicius, *Piezoelectric Multi-degree of Freedom Actuators/Sensors*, Proc. 3rd Int. Conf. Motion and Vibration Control, pp. K9-K15, 1996.

[4] T. Amano *et al.*, *An Ultrasonic Actuator with Multi-Degree of Freedom using Bending and Longitudinal Vibrations of a Single Stator.* Proc. IEEE Int. Ultrasonics Symp., pp.667-670, 1998.

[5] S. Toyama *et al.*, *Multi degree of freedom Spherical Ultrasonic Motor*, Proc. IEEE Int. Conf. Robotics and Automation, pp. 2935-2940, 1995.

[6] K. Sasae *et al.*, *Development of a Small Actuator with Three Degrees of Rotational Freedom (3rd report)*, J. Japan Society of Precision Engineering, Vol. 62, No. 4, pp. 599-603, 1996. [*in Japanese*]

[7] K. Takemura *et al.*, *A Master-Slave System Using a Multi-DOF Ultrasonic Motor and its Controller Designed Considering Measured and Simulated Driving Characteristics*, Proc. 2001 IEEE/RSJ Int. Conf. Intelligent Robots and Systems, pp. 1977-1982, 2000.

[8] T. Maeno *et al.*, *Finite Element Analysis of the Rotor/Stator Contact in Ring-Type Ultrasonic Motor*, IEEE Trans. Ultrasonic Ferroelectrics and Frequency Control, Vol. 39, No. 6, pp. 668-674, 1992.

[9] T. Maeno, *Contact analysis of traveling wave type ultrasonic motor considering stick/slip condition*, J. the Acoustical Society of Japan, Vol. 54, No. 4, pp. 305-311, 1998. [*in Japanese*]

[10] M. Kurosawa, and S. Ueha, *Efficiency of ultrasonic motor using traveling wave*, J. the Acoustical Society of Japan, Vol. 44, No. 1, pp. 40-46, 1988. [*in Japanese*]

[11] Faa-Jeng Lin *et al.*, *Identification and Control of Rotary Traveling-Wave Type Ultrasonic Motor Using Neural Networks*, IEEE Trans. Control Systems Technology, Vol. 9, No. 4, pp. 672-680, 2001.

Kenjiro Takemura received his B. S. degree in mechanical engineering and M. S. degree in biomedical engineering from Keio University, Yokohama, Japan, in 1998 and 2000, respectively. He is currently working towards the Ph. D. degree in integrated design engineering also at Keio University. He is a Research Fellow of the Japan Society for the Promotion of Science.

Takashi Maeno received his B. S. and M. S. degrees in mechanical engineering from the Tokyo Institute of Technology, Tokyo, Japan, in 1984 and 1986, respectively. From 1986 to 1995, he worked for Canon, Inc., in Tokyo, Japan. He was a Visiting Industrial Fellow at the University of California, Berkeley, from 1990 to 1992. He received his Ph. D. degree in mechanical engineering from the Tokyo Institute of Technology, Tokyo, Japan, in 1993. Since 1995, he has been with the Department of Mechanical Engineering at Keio University, Yokohama, Japan, where he is currently an Associate Professor. He was a Visiting Professor at Harvard University in 2001.